Journal of Alloys and Compounds 509 (2011) 4557–4562

Contents lists available at ScienceDirect

Journal of Alloys and Compounds

journal homepage: www.elsevier.com/locate/jallcom

Preparation of thermally stable anatase TiO_2 photocatalyst from $TiOF_2$ precursor and its photocatalytic activity

Kangle Lv[a,b], Jiaguo Yu[a,*], Longzhe Cui[b], Shulin Chen[b], Mei Li[b]

[a] State Key Laboratory of Advanced Technology for Material Synthesis and Processing, Wuhan University of Technology, Luoshi Road 122#, Wuhan 430070, China
[b] Key Laboratory of Catalysis and Materials Science of the State Ethnic Affairs Commission & Ministry of Education, South-Central University for Nationalities, Wuhan 430074, China

ARTICLE INFO

Article history:
Received 4 October 2010
Received in revised form 10 January 2011
Accepted 15 January 2011
Available online 22 January 2011

Keywords:
Titanium dioxide
Titanium oxydifluoride
Fluoride
Microwave synthesis
Thermal stablility
Photocatalytic activity

ABSTRACT

Preparation of anatase TiO_2 with high themal stability is of great importance for its environmental application. In this work, $TiOF_2$ was first synthesized by a simple microwave-assisted hydrothermal route using tetrabutyl titanate and hydrofluoric acid as precursors at 200 °C for 20 min. Then the resulted precipitates were calcined at different temperatures (300–1000 °C) for 2 h. The as-prepared samples were characterized by X-ray diffraction, Raman spectrum, scanning electron microscopy, N_2 adsorption–desorption isotherms and X-ray photoelectron spectroscopy. The photocatalytic activity was evaluated using Brilliant Red X3B, an anionic azo dye, as the target organic molecule under UV light irradiation. The results showed that the prepared $TiOF_2$ exhibited weak or no photocatalytic activity. The phase transformation of $TiOF_2$ to anatase TiO_2 occurred at about 300 °C. The prepared anatase TiO_2 from $TiOF_2$ showed very high thermal stability and the anatase-to-rutile phase transformation temperature was up to 1000 °C. Fluoride ions played an important role in the improvement of thermal stability of anatase TiO_2 by strongly adsorbing on the crystal planes of anatase to stabilize the anatase structure. The 700 °C-calcined sample showed the highest photocatalytic activity due to its relative good crystallization and high specific surface areas.

1. Introduction

In recent years, in order to solve the increasingly serious environmental pollution problems, heterogeneous semiconductor photocatalysis gradually becomes a popular technique for its potential to control aqueous contaminates or air pollutants [1–7]. Among various oxide semiconductor photocatalysts, titania has attracted increasing attention due to its biological and chemical inertness, strong photo oxidization power, cost effectiveness, and long-term stability against photo and chemical corrosion [1,8–14].

Now many proposed innovative and commercial applications for photocatalytically active stable titania-coated materials such as bathroom tiles, sanitary wares, and self-cleaning glass for the control of organic contaminants require high processing temperatures and hence high-temperature stability [13,14]. However, pure anatase is metastable and inclines to transform into rutile when heating temperature is higher than 600 °C owing to its higher surface energy than rutile, thus limiting its suitability for high-temperature applications [13,14]. Therefore, the increase of thermal stability temperature of anatase TiO_2 is of great importance in broadening the applications.

Most of the work reported to improve the thermal stability of anatase TiO_2 is to utilize metal ion doping [15]. One of the drawbacks of metal ion doping is the possible generation of secondary impurity phases which affects phase purity and thus reduces the photocatalytic activity of titania. Nonmetal elements, such as Si [16], P [16–18], S [13,19,20], N [13] and F [14,21], were also used as dopant or co-dopant of TiO_2 to extend the anatase-to-rutile phase transformation temperature. Xia et al. synthesized La and S elements co-doped TiO_2 photocatalyst [19]. They found that the doping of La^{3+} accelerated slightly the anatase-to-rutile phase transition. However, the co-doping of La^{3+} and S hindered the aggregation and growth of TiO_2 particles. The study of Yu et al. [17] showed that P and Zn co-doped TiO_2 nanoparticles not only can totally stabilize anatase-TiO_2 at 800 °C, but also exhibit superior photocatalytic abilities. It was also reported that the Si doped TiO_2 had its anatase structure stabilized at 700 °C, and P doped TiO_2 were able to preserve the anatase-TiO_2 at temperature as high as 900 °C [16].

Recently, doping TiO_2 with F has attracted great attentions to obtain high thermal stability of anatase TiO_2 [14,21,22]. The study of Yu et al. showed that doping TiO_2 with NH_4F not only enhanced the crystallization of anatase, but also prevented phase transition of anatase to rutile [22]. Padmanabhan et al. reported the preparation of high-temperature stable anatase titania (900 °C) by reaction of titanium tetraisopropoxide with trifluoroacetic acid, and they

* Corresponding author. Tel.: +86 27 87871029; fax: +86 27 87879468.
E-mail address: jiaguoyu@yahoo.com (J. Yu).

0925-8388/$ – see front matter © 2011 Elsevier B.V. All rights reserved.
doi:10.1016/j.jallcom.2011.01.103

attributed the improved thermal stability to the small amounts of fluorine in the lattice [12]. Lv et al. reported the preparation of F-doped titania nanoparticles by alcoholysis of $TiCl_4$ in the presence of NH_4F, which showed a high thermal stability temperature of up to 1000 °C [14]. All these studies mentioned above indicate that fluoride plays an important role in the enhanced thermal stability of anatase TiO_2. Instead of using F-doped TiO_2 as the starting materials, this paper studied the thermal stability of anatase TiO_2 prepared by calcination of the $TiOF_2$ precursor on considering that $TiOF_2$ contains much higher F-content (F/Ti = 2) than F-doped TiO_2 (F/Ti ≤ 0.1).

2. Experimental

2.1. Sample preparation

Tetrabutyl titanate (TBT) and hydrofluoric acid (40 wt.%) were used for the preparation of $TiOF_2$. Firstly, 40 mL of hydrofluoric acid solution was dropwise added into a beaker containing 100 g TBT under magnetic stirring. Then, the mixture was sealed in Teflon-lined double-walled digestion vessel. After treating at 200 °C for 20 min using a microwave digestion system (MDS-6, SINEO), the vessel was cooled down to room temperature. The white precipitates were filtrated, washed with deionised water and absolute ethanol for three times, and then dried in air. Finally, the obtained precipitates were calcined at 300, 400, 500, 600, 700, 800, 900 and 1000 °C for 2 h, respectively. For simplification, the resulted samples were labeled as T*x*, where *x* presents the sintering temperature. For example, T700 represented the powder that was sintered at 700 °C for 2 h in air (T200 represented the uncalcined $TiOF_2$).

2.2. Characterization

X-ray diffraction (XRD) patterns, obtained on a D/Max-RB X-ray diffractometer (Rigaku, Japan) using Cu Kα irradiation at a scan rate of 0.05° $2\theta\,S^{-1}$, were used to determine the phase structure of the obtained samples. Average crystallite size of TiO_2 was determined by XRD using Scherrer equation [22–25]. Raman spectrum was recorded at room temperature using a micro-Raman spectrometer (Renishaw InVia) in the backscattering geometry with a 514.5 nm Ar^+ laser as an excitation source. The morphology of the sample was observed on a field emission scanning electron microscope (SEM) (Hitachi, Japan) with an acceleration voltage of 10 kV. The Brunauer–Emmett–Teller surface area (S_{BET}) of the samples were analyzed by nitrogen adsorption in a Micromeritics ASAP 2020 nitrogen adsorption apparatus (USA), which was determined by a multipoint BET method using the adsorption data in the relative pressure (P/P_0) range of 0.05–0.3. Pore volume and average pore size (APS) were determined by nitrogen adsorption volume at the relative pressure of 0.994. Uncalcined and calcined samples were degassed at 180 °C prior to nitrogen adsorption measurements. X-ray photoelectron spectroscopy (XPS) measurements were performed by a Multilab 2000 XPS system with a monochromatic Mg K*α* source and a charge neutralizer. All of the binding energies were referenced to the C 1s peak at 285.0 eV of the surface adventitious carbon.

2.3. Photoactivity evaluation

Photocatalytic reactions were carried out using a high-pressure mercury lamp (375 W, Shanghai Yamin) as light source, emitted mainly at 365 nm. The reactor (80 mL) was made of a Pyrex glass, and positioned at a fixed distance of ca. 10 cm from the lamp. Reactive brilliant red X3B (X3B), an anionic organic dye, was used as the target organic pollutant (Fig. 1). Prior to illumination, a suspension containing 50.0 mg of catalyst and 50.0 mL of 1.0×10^{-4} mol/L X3B was continuously stirred in the dark for 12 h to establish the adsorption–desorption equilibrium. During the photoreaction, the reactor was thermostated at 25 °C through a water recycle system and stirred mechanically at a constant rate. At given intervals of illumination, small aliquots of the suspension were withdrawn by syringe, centrifuged, and then filtered through a Millipore filter (pore size 0.45 μm). The filtrates were monitored by a UV–vis spectroscopy (Lambda Bio 35, PE Co.) at 510 nm.

3. Results and discussion

3.1. Crystalline phase and morphology

The phase structure, crystallite size, and crystallinity of TiO_2 are of great importance for its photocatalytic activity. XRD was used to investigate the changes of phase structures and crystallite sizes of the photocatalyst. Fig. 2 shows the effects of calcination temperature on phase transformation of the precursor. As for the precursor (T200), all the diffraction peaks corresponding to $TiOF_2$ (JCPDS No. 01-0490) were observed and no peak of any TiO_2 phases (anatase and rutile) exists, which indicates that T200 is pure $TiOF_2$. The broad peak at $2\theta = 23.4°$ corresponds to the (1 0 0) plane diffraction of $TiOF_2$ (Fig. 2) [26]. However, when $TiOF_2$ precursor is calcined at 300 °C, the peak at $2\theta = 23.4°$ gradually disappears. Meanwhile, a broad peak at $2\theta = 25.3°$, corresponding to the diffraction peak of (1 0 1) plane of anatase TiO_2 (JCPDS No. 21-1272) [27,28], is formed (Fig. 2). When the calcination temperature increases to 400 °C, the peaks of $TiOF_2$ vanish and the peak intensity of anatase increases, indicating the complete phase transformation of $TiOF_2$ to anatase TiO_2. Further observation shows that with increasing the calcination temperatures from 300 to 900 °C, XRD peak intensities of anatase steadily become stronger and the width of XRD diffraction peaks of anatase becomes narrower, indicating the formation of highly crystalline larger TiO_2 crystallites [29].

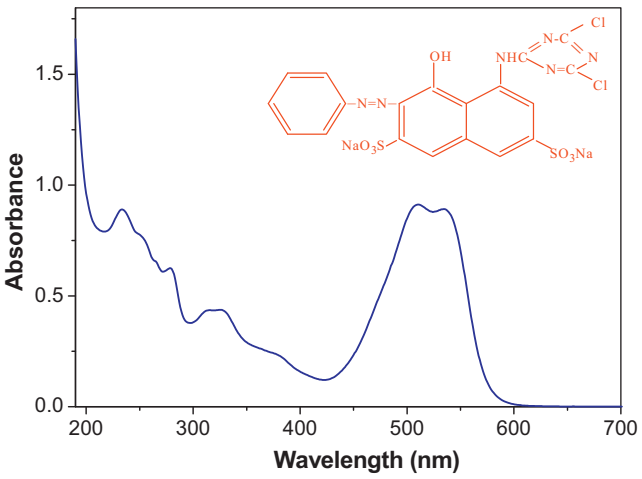

Fig. 1. Structure and electronic absorption spectrum of X3B in water.

Raman spectroscopy is widely employed in TiO_2 studies, as anatase and rutile polymorphs belong to different spaces groups and hence exhibit their characteristic Raman bands. Fig. 3 shows Raman spectrum of T900 sample, characteristic bands at 139.7, 391.6, 512.4 and 634.9 cm^{-1} correspond to the $E_{g(1)}$, $B_{1g(1)}$, $A_{1g} + B_{1g(2)}$ and $E_{g(2)}$ modes of anatase. Both the position and the relative intensity of the observed Raman bands are in good accordance with the position and the relative intensity of anatase reported in the literature [30,31]. Therefore, the phase purity of T900 is further confirmed.

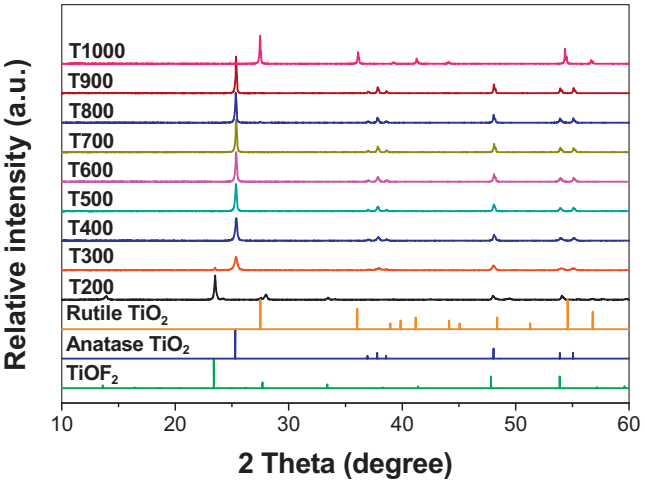

Fig. 2. XRD patterns of the photocatalysts, together with the expected diffraction peaks for anatase and rutile TiO_2, and $TiOF_2$, respectively.

Table 1
Physical properties of the photocatalysts.

Calcination temperature (°C)	Phase	Crystallite size (nm)	S_{BET} (m^2/g)	Pore volume (cm^3/g)	APS (nm)	Relative crystallinity
Precursor	$TiOF_2$	–	23.1	0.16	28.5	–
300	Anatase	29.6	15.9	0.13	39.5	1.00
400	Anatase	40.8	11.2	0.056	22.8	1.68
500	Anatase	49.6	9.5	0.027	11.1	2.02
600	Anatase	52.6	8.9	0.027	12.1	2.14
700	Anatase	54.3	6.6	0.018	16.2	2.22
800	Anatase	57.1	5.8	0.015	14.2	2.31
900	Anatase	61.5	4.0	–	–	2.56
1000	Rutile	80.0	0.8	–	–	–

The crystallinity of TiO_2 nanoparticles was quantitatively evaluated via the relative intensity of the (1 0 1) diffraction peak of the anatase [32,33]. Table 1 lists the average crystalline sizes and relative anatase crystallinity of TiO_2 samples calcined at different temperature. It can be seen that the average crystalline sizes and relative anatase crystallinity increase with increasing calcination temperature. With further increasing the calcination temperature to 1000 °C, pure rutile phase is obtained (Fig. 2). It has been well documented that without any modification, phase transformation of anatase to rutile usually occurs at ca. 600 °C [12,13,16,29,34]. In the present study, anatase TiO_2 prepared from $TiOF_2$ shows very high thermal stability temperature (900 °C) before being transformed into rutile phase.

The morphologies of T200 (precursor) and T700 powders were further studied by SEM. Fig. 4a and b shows the SEM images of the as-prepared $TiOF_2$ powders before calcination. It can be observed that $TiOF_2$ grains are in shapes of cube or nanorod, similar to the report in the literature [26]. Compared with that of T700 sample, the particle size distribution of $TiOF_2$ is obviously broader (Fig. 4a and c).

3.2. BET surface areas and pore size distributions

Nitrogen adsorption–desorption isotherms were used for texture analysis (Fig. 5). The isotherm corresponding to T200 is of type IV (Brunauer–Deming–Deming–Teller (BDDT) classification) with the hysteresis loop of type H3, indicating the presence of slit-like pores, which agrees well with their morphology (Fig. 4). The isotherms show high absorption at high relative pressure (P/P_0) range (approaching 1.0), indicating the formation of large mesopores and macropores, consistent with the pore size distribution curves (inset of Fig. 5). The existing nanopores (or pore volume) are from the aggregation of sheet-shaped grains. Such organized porous structures are extremely useful in photocatalysis as they will provide efficient transport pathways to reactant and product molecules [35,36]. With increase in the calcination temperature, the isotherms of the photocatalyst shift downward and the hysteresis loops at high relative pressure become smaller, indicating a decrease in BET surface areas and the pore volumes due to the growth of the crystallite. Table 1 shows quantitative details on BET surface areas, APS and pore volume of the TiO_2 samples calcined at different temperatures. It can be seen that the pore volume and BET surface area decrease with increasing the calcination temperatures. The BET surface areas of the samples decrease from 23.1 to 11.2 and 6.6 m^2/g, whilst the pore volumes decrease from 0.16 to 0.056 and 0.018 cm^3/g for T200, T400 and T700 samples, respectively. Note that the APS of T300 is larger than that of T500–800 samples. This is due to the fact that T300 is a mixed phase of anatase and $TiOF_2$ (Fig. 2). Compared with size of anatase TiO_2 nanoparticles, the particle size distribution of $TiOF_2$ is in a broader range (From Fig. 4, we can see that some cubic $TiOF_2$ particles are in size of 50–200 nm).

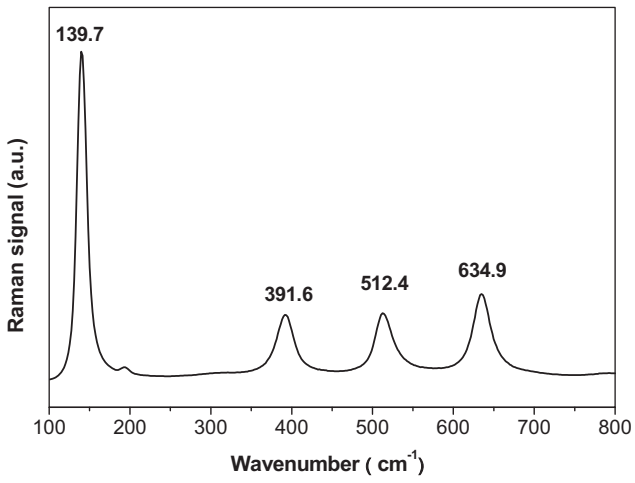

Fig. 3. Raman spectrum of T900.

3.3. XPS analysis

Fig. 6A shows XPS survey spectrum of a typical calcined TiO_2 sample (T700) compared with that of the as-synthesized precursor $TiOF_2$ (T200). Sharp photoelectron peaks appear at binding energies of 458 (Ti 2p) and 531 eV (O 1s) in both cases, along with a C 1s peak at 285 eV due to contamination from the XPS instrument itself. As expected, an additional peak at ca. 684 eV (F 1s) is found in the survey spectrum of the precursor $TiOF_2$ with an F/Ti molar ratio of 2.0, which further confirmed the formation of pure $TiOF_2$. The corresponding high-resolution XPS spectrum of F 1s region demonstrates that the F species in the $TiOF_2$ display only one peak of binding energy ca. 684.7 eV (Fig. 6B), which is a typical value for fluorated TiO_2 systems such as $TiOF_2$ or the surface Ti–F species [37]. The previously reported F-doped TiO_2 displayed two peaks around 684.3 and 688.4 eV for F 1s, which were respectively assigned to the F species adsorbed on the TiO_2 surface and those incorporated into the TiO_2 lattice [35]. Weak F 1s XPS signal at 684.6 eV was also detected for T700 sample (F/Ti = 0.4%), indicating that most of fluorine was eliminated upon calcination. According to the high-resolution XPS spectra of F 1s region shown in Fig. 6C, the F species in the T700 could also be assigned to F^- adsorbed on the surface of TiO_2, and no signal of F^- species that are incorporated into the TiO_2 lattice is detected.

Yu et al. studied the effects of F^- doping on the microstructures of nanocrystalline TiO_2 powders by hydrolysis of titanium tetraisopropoxide in a NH_4F aqueous solution [38], and found that the phase transformation of anatase-to-rutile is suppressed by the presence of F^- ions. Furthermore, the study of Lv et al. also showed that F^- increased the phase transformation temperature of anatase-to-rutile in F-doped TiO_2 sample prepared by alcoholysis of $TiCl_4$ in the presence of NH_4F [14]. The effect of fluoride on the thermal stability of anatase phase is due to the following causes: (1) F^- ions can be strongly adsorbed on the crystal planes of anatase and stabilize

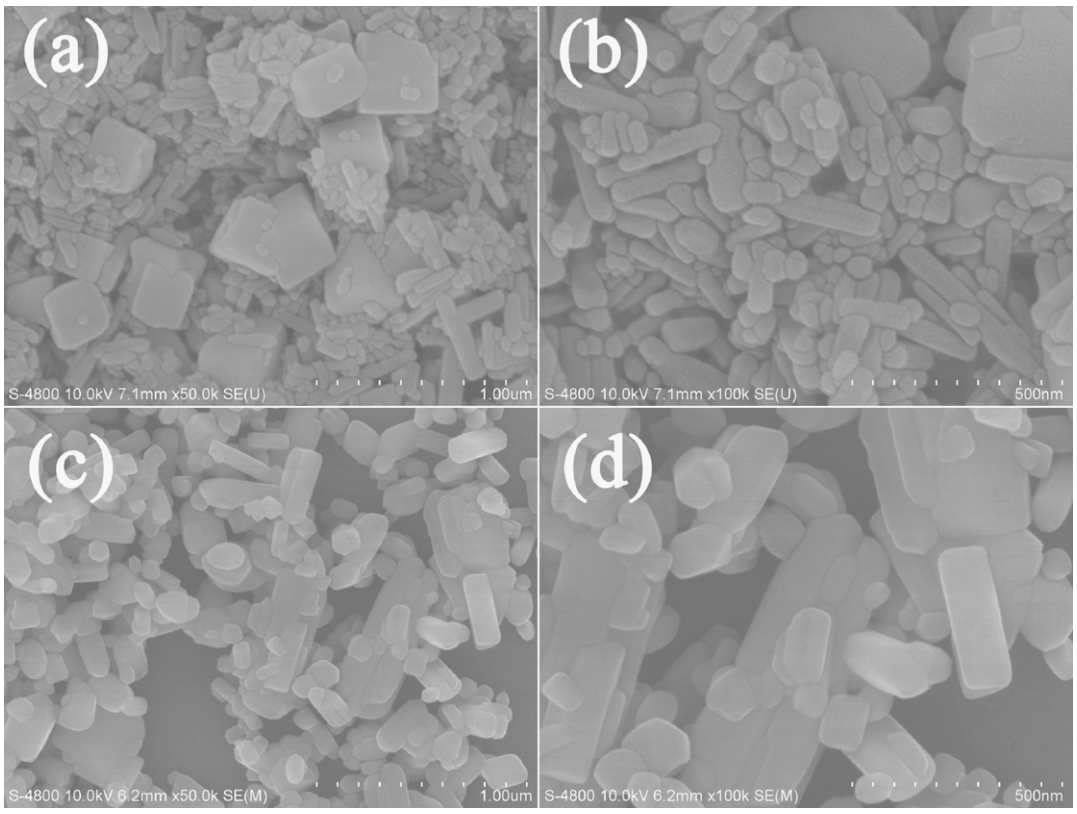

Fig. 4. SEM images of the precursor (a and b) and T700 sample (c and d).

the anatase phase structure to reduce the surface energy of anatase [14,37]. (2) The growth of anatase TiO_2 crystallites is restricted due to the adsorbed F^- ions on grain boundary, inhibiting the phase transformation of anatase to rutile [16]. (3) With increase in the calcination temperature, the adsorbed F^- ions are desorbed from the surface of TiO_2, resulting in the formation of vacancies. These vacancies also inhibit the growth of crystallites and the occurrence of anatase-to-rutile phase transformation.

3.4. Evaluation of photocatalytic activity

To study the effects of calcination temperatures on the photocatalytic activity of the photocatalyst, photocatalytic degradation of X3B was performed under UV irradiation ($\lambda \geq 320$ nm). Note that X3B is a very stable organic chemical and it shows little degradation under UV irradiation ($\lambda \geq 320$ nm) in the absence of photocatalyst [8,25,39,40]. Fig. 7 shows the dependence of X3B concentration on irradiation time in the presence of photocatalyst calcined at different temperatures. The kinetic data for the degradation of X3B can be well fitted by the apparent first-order rate equation, $\ln(C/C_0) = k_{app}t$, where k_{app} is rate constant, C and C_0 are the concentration of X3B at irradiation time $t = 0$ and t, respectively. Fig. 8 shows the effects of calcination temperatures on the degradation rate constants of X3B. Although $TiOF_2$ precursor has the largest specific surface areas (23.1 m^2/g) among all the photocatalysts (see Table 1), it shows the lowest photocatalytic activity with a rate constant of only 3.65×10^{-4} min^{-1} (Fig. 8). With increase in calcination temperature, the photocatalytic activity of anatase TiO_2 increases, and the highest photocatalytic activity is achieved for T700 (with a rate constant of 0.033 min^{-1}). This can be explained by the highly crystalline of anatase TiO_2 (Table 1) and the surface fluorinaton [8,25]. Usually, enhancement of crystallization is beneficial in reducing the combination of photo-generated electrons and holes [27,29,38–45], and thus the photocatalytic activity of TiO_2 is improved. Surface fluorination can also greatly enhance the photocatalytic activity of anatase TiO_2 since the $^{\bullet}OH$ radicals generated on the surface of F-TiO_2 are more mobile than those generated on pure TiO_2 under UV irradiation (Eqs. (1) and (2)) [25,35]:

$$\equiv Ti\text{–}OH + h_{vb}{}^{+} \rightarrow \equiv Ti\text{–}OH^{\bullet +}(^{\bullet}OH_{ads}) \quad (1)$$

$$\equiv Ti\text{–}F + H_2O + h_{vb}{}^{+} \rightarrow \equiv Ti\text{–}F + {}^{\bullet}OH_{free} + H^{+} \quad (2)$$

Therefore, the adsorbed fluoride ions on the surface of T700 also play an important role in the enhancement of the photocatalytic activity.

T800 shows similar photoactivity with T700 sample. This can be interpretated by their similar surface areas and crys-

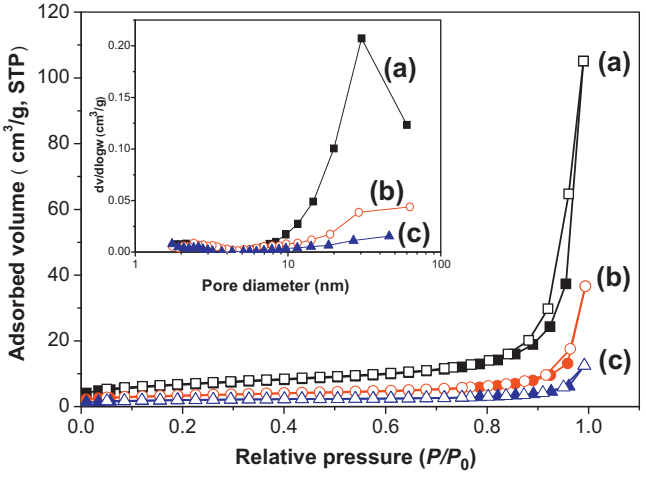

Fig. 5. Nitrogen adsorption–desorption isotherms and the corresponding pore size distributions (inset) of the precursor (a), T400 (b) and T700 (c).

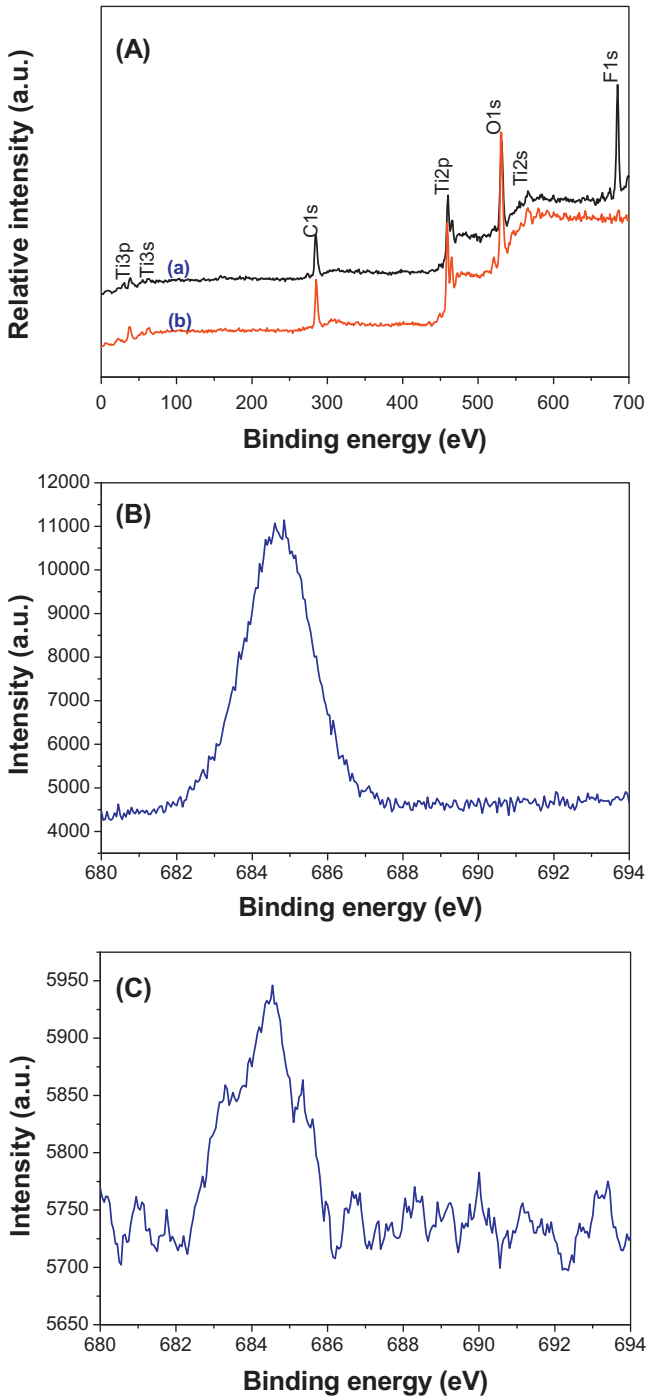

Fig. 6. XPS survey spectra (A) of the precursor (a) and T700 (b), and the corresponding high-resolution XPS spectra of F 1s region of the precursor (B) and T700 (C).

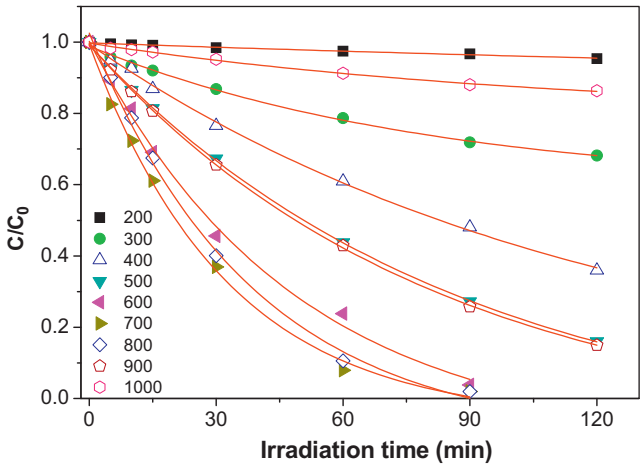

Fig. 7. Photocatalytic degradation of X3B under UV irradiation (TiO_2: 1.0 g/L, X3B: 1.0×10^{-4} mol/L, $\lambda \geq 320$ nm).

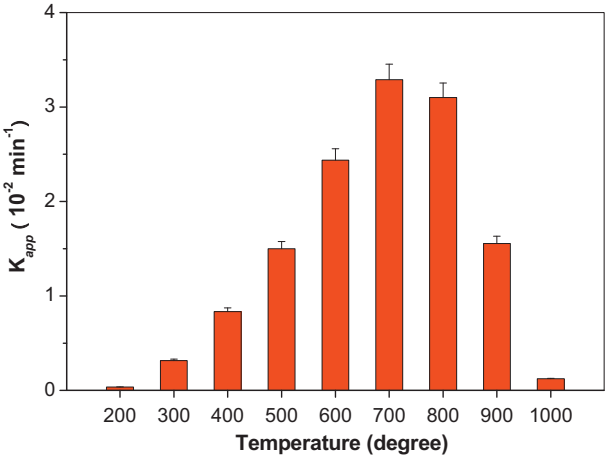

Fig. 8. Dependence of the photocatalytic activity on calcination temperature.

tallinity (Table 1). With further increasing calcination temperature to 900 °C, the photocatalytic activity of anatase TiO_2 samples decreases due to the decrease of specific surface areas and desorption of surface fluoride ions. The photocatalytic activity of T1000 sharply decreases (rate constant 0.0012 min^{-1}) because of the formation of rutile phase and decrease in specific surface areas (0.82 m^2/g) [24].

For comparison, the photocatalytic activity of commercial photocatalyst P25 (Degussa) is also tested under the same condition. The degradation rate constant of X3B in P25 is 0.047 min^{-1}, which seems higher than that of T700 (0.033 min^{-1}). However, the specific photocatalytic activity (per surface area unit) of T700 (0.0050 min^{-1} m^{-2}) is 5 times higher than that of P25 photocatalyst (0.0010 min^{-1} m^{-2}). This is because the specific surface area of P25 (45.0 m^2/g) is much larger than that of T700 (only 6.6 m^2/g).

4. Conclusions

In summary, a simple and novel synthetic method for the fabrication of $TiOF_2$ was developed via a microwave-assisted hydrothermal route using TBT and hydrofluoric acid as raw materials. The prepared anatase TiO_2 from $TiOF_2$ shows very high thermal stability and the phase transformation temperature from anatase to rutile is up to 1000 °C. Fluoride ions play an important role in the improvement of the thermal stability of anatase TiO_2 by strongly adsorbed on the surface of anatase and prevented its growth. The 700 °C-calcined anatase TiO_2 sample shows the highest photocatalytic activity due to its good crystallization and suitable specific surface areas. This study will provide new insight into design and preparation of advanced photocatalytic materials with high-temperature stability.

Acknowledgements

This work was partially supported by the National Natural Science Foundation of China (20977114, 50625208 and 20877061), China Postdoctoral Science Foundation (20090451086

and 201003500) and the Open Fund of the Key Laboratory of Catalysis and Materials Science of the State Ethnic Affairs Commission and Ministry of Education, Hubei Province (Grant CHCL09006).

References

[1] N. Todorova, T. Giannakopoulou, T. Vaimakis, C. Trapalis, Mater. Sci. Eng. B 152 (2008) 50–54.
[2] L. Zhang, A.J. Xie, Y.H. Shen, S.K. Li, J. Alloys Compd. 505 (2010) 579–583.
[3] M. Rezaee, S.M. Mousavi Khoie, J. Alloys Compd. 507 (2010) 484–488.
[4] W. Li, Y. Bai, C. Liu, Z.H. Yang, X. Feng, X.H. Lu, N.K. Laak, K.Y. Chan, Environ. Sci. Technol. 43 (2009) 5423–5428.
[5] A.M. El-Toni, S. Yin, T. Sato, T. Ghannam, M. Al-Hoshan, M. Al-Salhi, J. Alloys Compd. 508 (2010) 1–4.
[6] M. Lim, Y. Zhou, B. Wood, L.Z. Wang, V. Rudolph, G.Q. Lu, Environ. Sci. Technol. 43 (2009) 538–543.
[7] Y. Liu, L.F. Chen, J.C. Hu, J.L. Li, R. Richards, J. Phys. Chem. C 114 (2010) 1641–1645.
[8] K.L. Lv, J.G. Yu, K.J. Deng, J. Sun, Y.X. Zhao, D.Y. Du, M. Li, J. Hazard. Mater. 173 (2010) 539–543.
[9] Y.L. Liao, W.X. Que, Z.H. Tang, W.J. Wang, W.H. Zhao, J. Alloys Compd. 509 (2011) 1054–1059.
[10] H. Kitagawa, T. Kunisada, Y. Yamada, S. Kubo, J. Alloys Compd. 508 (2010) 582–586.
[11] K.V. Baijua, P. Periyat, P. Shajesh, W. Wunderlich, K.A. Manjumol, V.S. Smitha, K.B. Jaimy, K.G.K. Warrier, J. Alloys Compd. 505 (2010) 194–200.
[12] S.C. Padmanabhan, S.C. Pillai, J. Colreavy, S. Balakrishnan, D.E. McCormack, T.S. Perova, Y. Gunko, S.J. Hinder, J.M. Kelly, Chem. Mater. 19 (2007) 4474–4481.
[13] P. Periyat, D.E. McCormack, S.J. Hinder, S.C. Pillai, J. Phys. Chem. C 113 (2009) 3246–3253.
[14] Y.Y. Lv, L.H. Yu, H.Y. Huang, H.L. Liu, Y.Y. Feng, Appl. Surf. Sci. 255 (2009) 9548–9552.
[15] D.J. Reidy, J.D. Holmes, M.A. Morris, Ceram. Int. 32 (2006) 235–239.
[16] H.F. Yu, S.T. Yang, J. Alloys Compd. 492 (2010) 695–700.
[17] H.F. Yu, Z.W. Zhang, F.C. Hu, J. Alloys Compd. 465 (2008) 484–490.
[18] R.Y. Zheng, Y. Guo, C. Jin, J.L. Xie, Y.X. Zhu, Y.C. Xie, J. Mol. Catal. A 319 (2010) 46–51.
[19] H.L. Xia, H.S. Zhuang, D.C. Xiao, T. Zhang, J. Alloys Compd. 465 (2008) 328–332.
[20] P. Periyat, S.C. Pillai, D.E. McCormack, J.C. Colreavy, S.J. Hinder, J. Phys. Chem. C 112 (2008) 7644–7652.
[21] E.P. Lokshin, T.A. Sedneva, Russ. J. Appl. Chem. 79 (2006) 1238–1241.
[22] J.C. Yu, J.G. Yu, W. Ho, Z. Jiang, L.Z. Zhang, Chem. Mater. 14 (2002) 3808–3816.
[23] H.S. Zuo, J. Sun, K.J. Deng, R. Su, F.Y. Wei, D.Y. Wang, Chem. Eng. Technol. 30 (2007) 577–582.
[24] K.L. Lv, J.G. Yu, K.J. Deng, X.H. Li, M. Li, J. Phys. Chem. Solid 71 (2010) 519–522.
[25] K.L. Lv, X.F. Li, K.J. Deng, J. Sun, X.H. Li, M. Li, Appl. Catal. B 95 (2010) 383–392.
[26] J. Zhu, D.Q. Zhang, Z.F. Bian, G.S. Li, Y.N. Huo, Y.F. Lu, H.X. Li, Chem. Commun. (2009) 5394–5396.
[27] J.G. Yu, Y.R. Su, B. Cheng, Adv. Funct. Mater. 17 (2007) 1984–1990.
[28] M.H. Zhou, J.G. Yu, S.W. Liu, P.C. Zhai, B.B. Huang, Appl. Catal. B 89 (2009) 160–166.
[29] J.G. Yu, H.G. Yu, B. Cheng, X.J. Zhao, J.C. Yu, W.K. Ho, J. Phys. Chem. B 103 (2003) 13871–13879.
[30] J.G. Li, T. Ishigaki, X.D. Sun, J. Phys. Chem. C 111 (2007) 4969–4976.
[31] Y.B. Mao, S.S. Wong, J. Am. Chem. Soc. 128 (2006) 8217–8226.
[32] J.G. Yu, W.G. Wang, B. Cheng, B.L. Su, J. Phys. Chem. C 113 (2009) 6743–6750.
[33] T. Ozawa, M. Iwasaki, H. Tada, T. Akita, K. Tanaka, S. Ito, J. Colloid Interface Sci. 281 (2005) 510–513.
[34] H. Kominami, M. Kohno, Y. Takada, M. Inoue, T. Inui, Y. Kera, Ind. Eng. Chem. Res. 38 (1999) 3925–3931.
[35] Q.J. Xiang, K.L. Lv, J.G. Yu, Appl. Catal. B 96 (2010) 557–564.
[36] S.W. Liu, J.G. Yu, J. Solid State Chem. 181 (2008) 1048–1055.
[37] H.G. Yang, C.H. Sun, S.Z. Qiao, J. Zou, G. Liu, S.C. Smith, H.M. Cheng, G.Q. Lu, Nature 453 (2008) 638–641.
[38] J.C. Yu, W.K. Ho, J.G. Yu, S.K. Hark, K. Iu, Langmuir 19 (2003) 3889–3896.
[39] K.L. Lv, Y.M. Xu, J. Phys. Chem. B 110 (2006) 6204–6212.
[40] X.F. Li, K.L. Lv, K.J. Deng, J.F. Tang, R. Su, J. Sun, L.Q. Chen, Mater. Sci. Eng. B 158 (2009) 40–47.
[41] K.L. Lv, C.S. Lu, Chem. Eng. Technol. 31 (2008) 1272–1276.
[42] Y.M. Xu, K.L. Lv, Z.G. Xiong, W.H. Leng, W.P. Du, D.L. Liu, X.J. Xue, J. Phys. Chem. C 111 (2007) 19024–19032.
[43] M.H. Zhou, J.G. Yu, J. Hazard. Mater. 152 (2008) 1229–1236.
[44] J.G. Yu, L.J. Zhang, B. Cheng, Y.R. Su, J. Phys. Chem. C 111 (2007) 10582–10589.
[45] S.W. Liu, J.G. Yu, M. Jaroniec, J. Am. Chem. Soc. 132 (2010) 11914–11916.